Cramér-Rao Bounds for the Simultaneous Estimation of Power System Electromechanical Modes and Forced Oscillations

Luke Dosiek
Department of Electrical, Computer & Biomedical Engineering
Union College
Schenectady, NY 12309
Emails: dosiekl@union.edu

***Abstract*—In this paper, the Cramér-Rao Bounds (CRB) for the simultaneous estimation of power system electromechanical modes and forced oscillations (FO) are derived. Two cases are considered; in the first case only the steady-state response to the FO is present in the measured system output used by estimation algorithms. In the second, the startup transient of the FO is present in addition to the steady-state response. The CRBs are analyzed numerically to explore sensitivities to FO frequency, signal-to-noise ratio (SNR) and observation window length. It is demonstrated that 1) the CRB of FO parameters is not affected by the presence of the transient response, 2) the CRB of the system modes is not affected by the presence of an FO in steady-state and 3) the CRB of the system modes can be drastically reduced by the presence of a FO startup transient.**

I. Introduction

The ability to estimate electromechanical modes as accurately as possible during a forced oscillation (FO) event is a critical task due to the potential for mode meters to model the FO as a system mode and throw false alarms on low damping [1]. With the ever-increasing penetration of inverter-based generation and microgrids, the potential for FOs is also increasing [2], while traditional power system components continue to cause FOs such as the 2019 system-wide event in the United States Eastern Interconnection [3].

A highly useful tool for assessing the accuracy of an estimation algorithm is the Cramér-Rao Bound (CRB), which defines the theoretical lower limit on the variance of an unbiased estimator. The CRB may be used as a benchmark with which to compare the variance of potential mode meters and FO parameter estimators before a particular method is selected for use. Additionally, analysis of the CRBs may yield insight into the underlying processes being estimated. Such a study was completed for mode meters under purely ambient conditions in [4], while the authors of [5] and [6] considered the case where unknown FOs were present in a known power system.

This paper considers the practical case where neither the FO nor the system parameters are known. After a brief review of small-signal power system modeling, the CRBs for FO parameters and mode frequency and damping are derived for two specific cases: one where only the steady-state response to the FO is present, and one that includes the FO startup transient. A simulation study is conducted that reveals several interesting observations, the most important of which is that the presence of transients associated with the onset of a FO can drastically increase the accuracy of electromechanical mode meters.

This material is based upon work supported by the National Science Foundation under Grant No. 1944689

II. System Models

It is well-known that for the purposes of electromechanical mode meters and oscillation monitoring systems where preprocessed PMU data are used (e.g., lowpass filtered and detrended bus voltage angle differences), a power system under ambient conditions is well-modeled with an autoregressive moving average (ARMA) structure. When N samples of y are collected at sampling rate f_s, they are indexed from $k = 0$ to $k = N - 1$ with the k^{th} sample of system output y given as

$$y[k] = \frac{C(q)}{A(q)}e[k] = \frac{1 + c_1 q^{-1} + \cdots + c_{n_c} q^{n_c}}{1 + a_1 q^{-1} + \cdots + a_{n_a} q^{n_a}} e[k] \tag{1}$$

where $A(q)$ and $C(q)$ are the AR and MA polynomials in delay operator q such that $q^{-n}y[k] = y[k - n]$, and e is Gaussian White Noise (GWN) attributed to low-level random load variations. The electromechanical mode frequency and damping are computed from the system poles, i.e., the n_a roots of $A(q)$. For the i^{th} pole p_i, the modal frequency in Hz and percent damping are found as

$$f_{mi} = \frac{\mathfrak{Im}(f_s \log p_i)}{2\pi} \tag{2}$$

$$\zeta_{mi} = -\cos\left(\angle f_s \log p_i\right) \times 100\% \tag{3}$$

Note that in (1), e is the only system input being modeled. When FOs are present in y, the autoregressive moving average with exogenous input (ARMAX) model may be used:

$$y[k] = \frac{B(q)}{A(q)}u[k] + \frac{C(q)}{A(q)}e[k] \tag{4}$$

where $B(q) = b_o + b_1 q^{-1} + \cdots + b_{n_b} q^{n_b}$ is the X polynomial and u, the input FO, is in the general the sum of p cosines

$$u[k] = \sum_{i=1}^{p} \tilde{A}_i \cos\left(\omega_i k + \tilde{\phi}_i\right) I_{\epsilon_i,\eta_i}[k] \tag{5}$$

where $\tilde{A}$, $\tilde{\phi}_i$, and ω_i are amplitude, phase in radians, and frequency in radians per sample. Recall that frequency in Hz is related to radians per sample by $f_i = \omega_i f_s/(2\pi)$. Function I defines the FO starting and ending samples, ϵ_i and η_i, as

$$I_{\epsilon_i,\eta_i}[k] = \begin{cases} 1, & \epsilon_i \le k \le \eta_i \\ 0, & \text{else} \end{cases} \tag{6}$$

Note that in reality the sources of these FOs are very much a part of the power system, despite the use of the word "exogenous" in the ARMAX acronym. For the remainder of this paper, in order to simplify derivations and analysis, only a single FO ($p = 1$) is considered. Extensions to multiple FOs are straightforward.

The FO observed in output y depends on when the FO starts and stops. This paper considers two specific cases. In case 1, the FO starts long before the first observation of y, and lasts throughout the entirety of the data record. In this case, only the steady-state response of the FO is present in y:

$$y[k] = A_1 \cos(\omega_1 k + \phi_1) + \frac{C(q)}{A(q)} e[k] \tag{7}$$

where amplitude and phase of the output FO are

$$A_1 = \frac{|B(\omega_1)|}{|A(\omega_1)|} \tilde{A}_1 \tag{8}$$

$$\phi_1 = \tilde{\phi}_1 + \angle B(\omega_1) - \angle A(\omega_1) \tag{9}$$

In case 2, the FO again lasts throughout the entirety of the data record, however it starts precisely at the first sample of y. Thus, y becomes

$$\begin{aligned} y[k] &= \frac{B(q)}{A(q)} \tilde{A}_1 \cos(\omega_1 k + \tilde{\phi}_1) + \frac{C(q)}{A(q)} e[k] \\ &= \sum_{i=1}^{n_a} r_i p_i^k + A_1 \cos(\omega_1 k + \phi_1) + \frac{C(q)}{A(q)} e[k] \end{aligned} \tag{10}$$

where r_i are residue terms that depend upon both the FO parameters and the coefficients of $B(q)$ and $A(q)$ and p_i are the poles of $A(q)$. While both (7) and (10) contain the same ARMA process and steady-state FO response, only (10) contains the FO startup transient response, $\sum_{i=1}^{n_a} r_i p_i^k$. It is demonstrated later that this additional term can have a profound effect on the CRB of the mode meter frequency and damping estimators.

The polynomial coefficients and FO parameters of models (7) and (10) may be collected in a vector termed θ_o. Estimating these parameters from observations of y involves minimizing a cost function of *prediction errors*, which are defined as

$$\varepsilon(k, \hat{\theta}) = y[k] - \hat{y}(k, \hat{\theta}) \tag{11}$$

where $\hat{\theta}$ is an estimate of θ_o and *predictor* $\hat{y}$ is the estimate of y for a particular $\hat{\theta}$. The prediction errors are thus estimates of the random system input e. Indeed, $\varepsilon(k, \theta_o) = e[k]$.

III. Asymptotic Cramér-Rao Bounds

In [7], a general expression for the asymptotic CRB of a dynamical system is given as

$$\mathrm{Cov}(\hat{\theta}) \ge \frac{\sigma_e^2}{N} \left[\frac{1}{N} \sum_{k=0}^{N-1} \mathrm{E}\left\{ \psi(k, \theta_o) \psi^T(k, \theta_o) \right\} \right]^{-1} \tag{12}$$

where E is the expected value operation, σ_e^2 is the variance of e, and ψ is gradient

$$\psi(k, \theta_o) = \frac{d}{d\theta} \hat{y}(k, \theta_o) \tag{13}$$

In practice, the expected value operation in (12) must be approximated numerically by averaging over M Monte Carlo simulations, each using statistically independent realization of e. The approximate CRB is

$$\mathrm{Cov}(\hat{\theta}) \gtrapprox \frac{\sigma_e^2}{N} \left[\frac{1}{N} \sum_{k=0}^{N-1} \frac{1}{M} \sum_{i=1}^{M} \left\{ \psi_i(k, \theta_o) \psi_i^T(k, \theta_o) \right\} \right]^{-1} \tag{14}$$

where $\psi_i(k, \theta)$ is the gradient vector from the i^{th} Monte Carlo trial. In practice, $M = 1000$ Monte Carlo trials is more than sufficient to observe convergence in the average.

Finally, note that the electromechanical mode frequency and damping are secondary parameters. They do not appear in θ_o, but are are functions of some of the elements of θ_o. In order to find the CRB for these, the Taylor Series method used in [4] may be applied.

In the following two subsections, the CRB are derived for the cases defined in (7) and (10).

A. Case 1

Here only the steady-state FO response is present in y. Rewriting expression (7) as

$$A(q) y[k] = A(q) A_1 \cos(\omega_1 k + \phi_1) + C(q) e[k] \tag{15}$$

leads to

$$\begin{aligned} \hat{y}(k, \theta_o) = &- \sum_{i=1}^{n_a} a_i y[k-i] + \sum_{i=1}^{n_c} c_i \varepsilon(k-i, \theta_o) \\ &+ \sum_{i=0}^{n_a} a_i A_1 \cos(\omega_1 (k-1) + \phi_1) \end{aligned} \tag{16}$$

where

$$\theta_o = \begin{bmatrix} a_1 & \cdots & a_{n_a} & c_1 & \cdots & c_{n_c} & A_1 & \phi_1 & \omega_1 \end{bmatrix}^T \tag{17}$$

The resultant gradient vector is

$$\begin{aligned} \psi(k, \theta_o) = \Bigg[&\frac{\partial \hat{y}(k, \theta_o)}{\partial a_1} \quad \cdots \quad \frac{\partial \hat{y}(k, \theta_o)}{\partial a_{n_a}} \\ &\frac{\partial \hat{y}(k, \theta_o)}{\partial c_1} \quad \cdots \quad \frac{\partial \hat{y}(k, \theta_o)}{\partial c_{n_c}} \\ &\frac{\partial \hat{y}(k, \theta_o)}{\partial A_1} \quad \frac{\partial \hat{y}(k, \theta_o)}{\partial \phi_1} \quad \frac{\partial \hat{y}(k, \theta_o)}{\partial \omega_1} \Bigg]^T \end{aligned} \tag{18}$$

with elements

$$\frac{\partial \hat{y}(k,\theta_o)}{\partial a_i} = \frac{1}{C(q)} A_1 \cos(\omega_1(k-i)+\phi_1) - \frac{1}{C(q)} y[k-i] \tag{19}$$

$$\frac{\partial \hat{y}(k,\theta_o)}{\partial c_i} = \frac{1}{C(q)} \varepsilon(k-i,\theta_o) \tag{20}$$

$$\frac{\partial \hat{y}(k,\theta_o)}{\partial A_1} = \frac{A(q)}{C(q)} \cos(\omega_1 k+\phi_1) \tag{21}$$

$$\frac{\partial \hat{y}(k,\theta_o)}{\partial \phi_1} = \frac{A(q)}{C(q)} (-A_1 \sin(\omega_1 k+\phi_1)) \tag{22}$$

$$\frac{\partial \hat{y}(k,\theta_o)}{\partial \omega_1} = \frac{A(q)}{C(q)} (-A_1 k \sin(\omega_1 k+\phi_1)) \tag{23}$$

where the details of the derivative calculations have been omitted due to space constraints.

Thus, finding the CRB of $\hat{\theta}$ for a particular ARMA model and FO involves the following steps. First, M independent N-sample sequences of e are generated and used to create M realizations of y. These, along with the sinusoids in (19) - (23), are filtered through $1/C(q)$ or $A(q)/C(q)$ to obtain the M realizations of ψ that are used by (14) to obtain the CRB. A subtle but very important detail here is that since y *only* contains steady-state FO responses, care must be taken to ensure that *only* the steady-state responses to the filtering operations in (19) - (23) are included in the gradient vectors.

The CRB of A_1, ϕ_1 and ω_1 are found as the final three diagonal elements of the CRB of $\hat{\theta}$, and the CRB of the mode frequency and damping are obtained by applying the the CRB of the AR polynomial coefficients (the $n_a \times n_a$ upper left block of the CRB of $\hat{\theta}$) to the methods found in [4].

B. Case 2

Rewriting (10),

$$\hat{y}(k,\theta_o) = -\sum_{i=1}^{n_a} a_i y[k-i] + \sum_{i=1}^{n_c} c_i \varepsilon(k-i,\theta_o) + \sum_{i=0}^{n_b} b_i \tilde{A}_1 \cos(\omega_1(k-1)+\tilde{\phi}_1) \tag{24}$$

with

$$\theta_o = \begin{bmatrix} a_1 & \cdots & a_{n_a} & b_0 & \cdots & b_{n_b} & c_1 & \cdots & c_{n_c} & \tilde{A}_1 & \tilde{\phi}_1 & \omega_1 \end{bmatrix}^T \tag{25}$$

and

$$\psi(k,\theta_o) = \begin{bmatrix} \frac{\partial \hat{y}(k,\theta_o)}{\partial a_1} & \cdots & \frac{\partial \hat{y}(k,\theta_o)}{\partial a_{n_a}} \\ \frac{\partial \hat{y}(k,\theta_o)}{\partial b_0} & \cdots & \frac{\partial \hat{y}(k,\theta_o)}{\partial b_{n_b}} \\ \frac{\partial \hat{y}(k,\theta_o)}{\partial c_1} & \cdots & \frac{\partial \hat{y}(k,\theta_o)}{\partial c_{n_c}} \\ \frac{\partial \hat{y}(k,\theta_o)}{\partial \tilde{A}_1} & \frac{\partial \hat{y}(k,\theta_o)}{\partial \tilde{\phi}_1} & \frac{\partial \hat{y}(k,\theta_o)}{\partial \omega_1} \end{bmatrix}^T \tag{26}$$

with elements

$$\frac{\partial \hat{y}(k,\theta_o)}{\partial a_i} = \frac{1}{C(q)} (-y[k-i]) \tag{27}$$

$$\frac{\partial \hat{y}(k,\theta_o)}{\partial b_i} = \frac{1}{C(q)} \tilde{A}_1 \cos(\omega_1(k-i)+\tilde{\phi}_1) \tag{28}$$

$$\frac{\partial \hat{y}(k,\theta_o)}{\partial c_i} = \frac{1}{C(q)} \varepsilon(k-i,\theta_o) \tag{29}$$

$$\frac{\partial \hat{y}(k,\theta_o)}{\partial \tilde{A}_1} = \frac{B(q)}{C(q)} \cos(\omega_1 k+\tilde{\phi}_1) \tag{30}$$

$$\frac{\partial \hat{y}(k,\theta_o)}{\partial \tilde{\phi}_1} = \frac{B(q)}{C(q)} (-\tilde{A}_1 \sin(\omega_1 k+\tilde{\phi}_1)) \tag{31}$$

$$\frac{\partial \hat{y}(k,\theta_o)}{\partial \omega_1} = \frac{B(q)}{C(q)} (-\tilde{A}_1 k \sin(\omega_1 k+\tilde{\phi}_1)) \tag{32}$$

Similar to Case 1, M independent realizations of e are created and applied to (10) to generate M independent realizations of y, both of which are filtered by $1/C(q)$ or $B(q)/C(q)$ along with the sinusoids of (27) - (32) to create M realizations of ψ that are used by (14) to obtain the CRB. Here, the subtle but important note is that since y *does* contain the start-up transient responses of the FO, so to should the gradient elements.

Note that in this case, while θ_o contains the FO frequency common to both the input and output FO, it only contains the amplitude and phase of the *input* FO. Thus, while the CRB of ω_1 is found as the last diagonal element of the CRB of $\hat{\theta}$, the CRB of A_1 and ϕ_1 must be obtained by applying Taylor Series linearizations to the CRB of $\hat{\theta}$.

Referring back to (8) and (9), define X as the phasor representation of the output FO

$$X = A_1 e^{j\phi_1} = \frac{B(\omega_1)}{A(\omega_1)} \tilde{A}_1 e^{j\tilde{\phi}_1} = \alpha + j\beta \tag{33}$$

where α and β are the real and imaginary parts of X. First, the CRB of $\begin{bmatrix}\alpha & \beta\end{bmatrix}^T$ is found from the CRB of $\hat{\theta}$ as

$$\text{Cov}\begin{bmatrix}\alpha \\ \beta\end{bmatrix} = J_{\alpha\beta} \text{Cov}(\hat{\theta}) J_{\alpha\beta}^T \tag{34}$$

where the Jacobian is obtained from the real and imaginary parts of complex Jacobian J_X

$$J_{\alpha\beta} = \begin{bmatrix} \mathfrak{Re}(J_X) \\ \mathfrak{Im}(J_X) \end{bmatrix} \tag{35}$$

where

$$J_X = \begin{bmatrix} \frac{\partial X}{\partial a_1} & \cdots & \frac{\partial X}{\partial a_{n_a}} & \frac{\partial X}{\partial b_0} & \cdots & \frac{\partial X}{\partial b_{n_b}} \\ \frac{\partial X}{\partial c_1} & \cdots & \frac{\partial X}{\partial c_{n_c}} & \frac{\partial X}{\partial \tilde{A}_1} & \frac{\partial X}{\partial \tilde{\phi}_1} & \frac{\partial X}{\partial \omega_1} \end{bmatrix} \tag{36}$$

with elements

$$\frac{\partial X}{\partial a_i} = \frac{-e^{-ji\omega_1}B(\omega_1)}{A^2(\omega_1)}\tilde{A}_1 e^{j\tilde{\phi}_1} \tag{37}$$

$$\frac{\partial X}{\partial b_i} = \frac{e^{-ji\omega_1}}{A(\omega_1)}\tilde{A}_1 e^{j\tilde{\phi}_1} \tag{38}$$

$$\frac{\partial X}{\partial c_i} = 0 \tag{39}$$

$$\frac{\partial X}{\partial \tilde{A}_1} = \frac{B(\omega_1)}{A(\omega_1)} e^{j\tilde{\phi}_1} \tag{40}$$

$$\frac{\partial X}{\partial \tilde{\phi}_1} = \frac{B(\omega_1)}{A(\omega_1)} j\tilde{A}_1 e^{j\tilde{\phi}_1} \tag{41}$$

$$\frac{\partial X}{\partial \omega_1} = \frac{B(\omega_1)\sum_{i=0}^{n_a} i a_i e^{-ji\omega_1} - A(\omega_1)\sum_{i=0}^{n_b} i b_i e^{-ji\omega_1}}{A^2(\omega_1)} \times \tilde{A}_1 e^{j\tilde{\phi}_1} \tag{42}$$

The CRB of $\begin{bmatrix} A_1 & \phi_1 \end{bmatrix}^T$ is then found from the CRB of $\begin{bmatrix} \alpha & \beta \end{bmatrix}^T$ as

$$\text{Cov}\begin{bmatrix} A_1 \\ \phi_1 \end{bmatrix} = J_{A\phi}\text{Cov}\begin{bmatrix} \alpha \\ \beta \end{bmatrix} J_{A\phi}^T \tag{43}$$

with Jacobian

$$J_{A\phi} = \begin{bmatrix} \frac{\partial A_1}{\partial \alpha} & \frac{\partial A_1}{\partial \beta} \\ \frac{\partial \phi_1}{\partial \alpha} & \frac{\partial \phi_1}{\partial \beta} \end{bmatrix} = \frac{1}{A_1}\begin{bmatrix} A_1\cos(\phi_1) & A_1\sin(\phi_1) \\ -\sin(\phi_1) & \cos(\phi_1) \end{bmatrix} \tag{44}$$

Finally, the CRBs of A_1 and ϕ_1 are the diagonal elements of (43), and as with Case 1, the CRB of the mode frequency and damping are obtained from applying the Taylor Series methods of [4] to the $n_a \times n_a$ upper left block of the CRB of $\hat{\theta}$).

IV. Simulation Study

To illustrate how FO parameters may affect system identification accuracy, a simulation study was conducted using a low-order ARMAX approximation of the minniWECC model. Details on the full minniWECC model are found in [8]. As was initially demonstrated in [4], when a single output of the minniWECC model is preprocessed by detrending, lowpass filtering and downsampling from 120 samples per second to 3, only a few of the system dynamics remain. The resulting process is very well-modeled as a low-order ARMAX system. Here, simulations were conducted with AR and MA orders of 10, and an X order of 1. The power spectral density (PSD) of the ARMA portion of the system is shown in Fig. 1, where the local maxima correspond to system modes that range from 0.21 Hz to 0.69 Hz. Here the main North-South interarea mode at 0.372 Hz and 4.67% damping was considered for estimation.

For each of the two FO cases, four scenarios were considered while the output FO amplitude and phase were held at $A_1 = 1$ and $\phi_1 = 0.8$ rad throughout. In the first scenario, the CRBs were calculated over a range of FO frequencies while the noise variance σ_e^2 was adjusted to maintain a constant local signal-to-noise ratio (SNR) of 40 dB. Local SNR is defined with the output FO as the signal and the PSD of the ARMA process *at only the FO frequency* as the noise power. The second scenario also found the CRBs over a range of FO frequencies, however a constant global SNR of 9.5 dB was maintained, where global SNR uses the average of the ARMA PSD across *the entire frequency range* as the noise power. In the third scenario, the CRBs were found over a range of global SNR while the FO frequency was held at 0.353 Hz. Finally, in the fourth scenario, the CRBs were found over a variety of record lengths while the FO frequency and global SNR were held at 0.353 Hz and 9.5 dB. Note that the first three scenarios used record lengths of 30 minutes, chosen somewhat arbitrarily since the CRBs are all inversely proportional to record length.

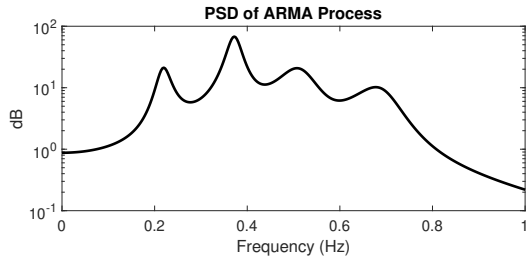

Fig. 1. Power spectral density of the ARMA system used in the simulations.

Results for the FO parameters are shown in Fig. 2. First note that in all four scenarios, the CRBs for the two FO cases were nearly identical to each other. This suggests that **the presence of the FO transient response has little effect on the ability to estimate its steady-state parameters.** Aside from that, the results are to be expected. In the leftmost plots, it is illustrated that the the CRB are nearly independent of FO frequency when local SNR is held constant, while they reflect the shape of the ARMA PSD (Fig. 1) when global SNR is held. Both of the rightmost plots demonstrate that the CRBs decrease as global SNR or record length increase, albeit at different rates.

Results for the CRBs of the mode frequency and damping are shown in Fig. 3. Note that in all four scenarios the CRBs from case 1 are nearly identical to those from purely ambient conditions (no FO). This implies that **when only the FO steady-state is present in the measured output, the FO has little effect on the CRB of the mode meter.** The case 2 results tell a different story. In the leftmost plots, a slight decrease in CRB was observed when the FO frequency was near the 0.372 Hz mode frequency, while a large drop in CRB was observed for FO frequencies outside the 0.2 to 0.7 Hz range of mode frequencies. There, the amplitude of the 0.372 Hz component of the FO transient response was especially large, providing a high energy ringdown in the data. In the rightmost plots, it was observed that the CRBs decreased with increasing global SNR or record length, the former of which can also be attributed to increasing amplitude in the 0.372 Hz component of the transient. This indicates that since the onset of a FO excites the system modes, **including FO startup transients in an analysis window can improve mode estimation accuracy.**

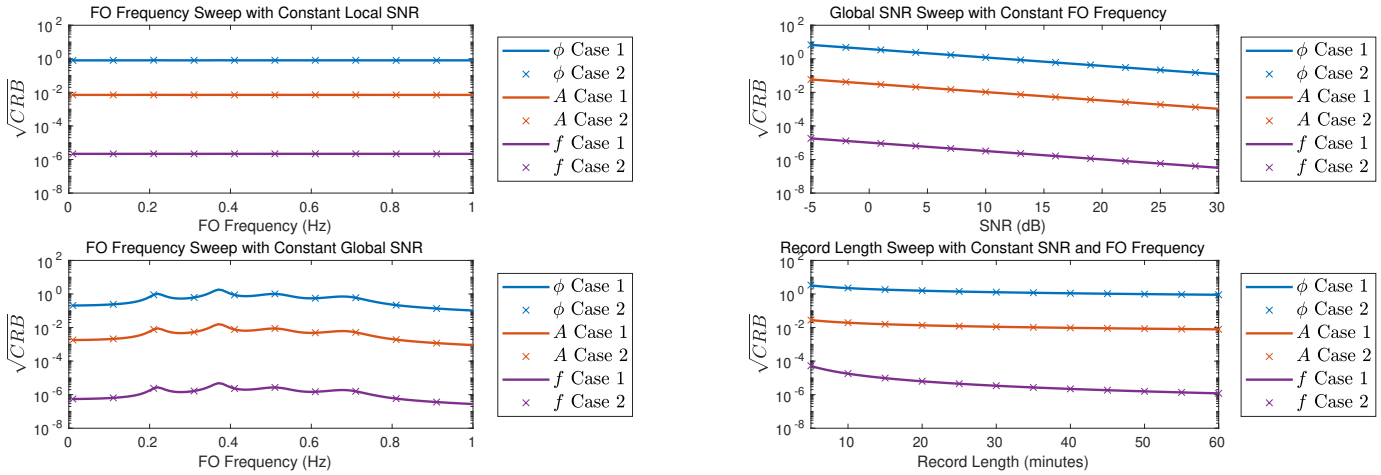

Fig. 2. Square root CRB of FO parameters for both FO cases as a function of FO frequency with constant local SNR (upper left), as a function of FO frequency with constant global SNR (lower left), as a function of global SNR with constant FO frequency (upper right), and as a function of record length with constant SNR and FO frequency (lower right).

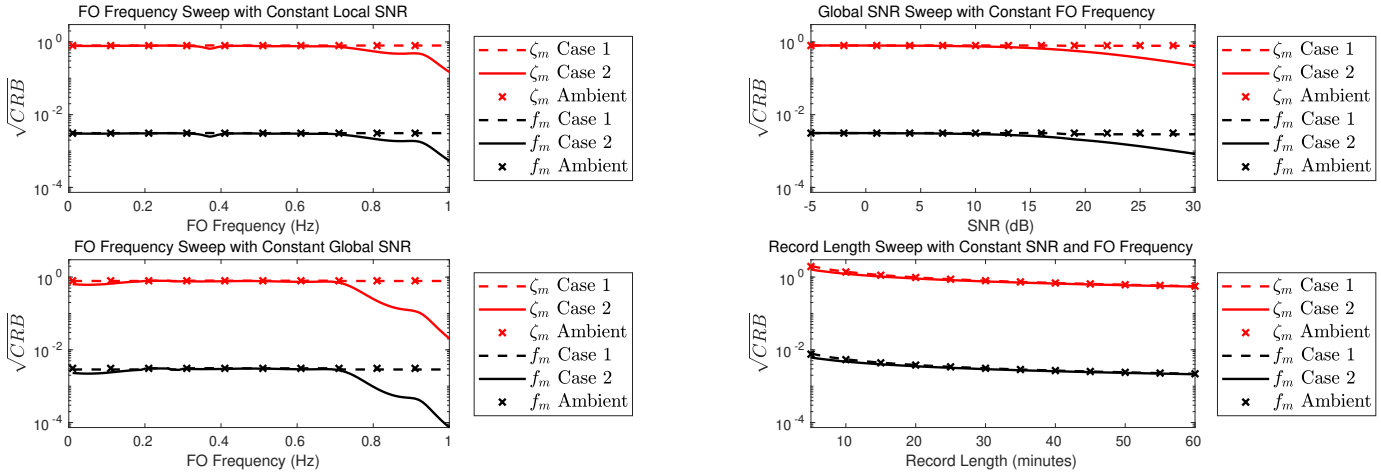

Fig. 3. Square root CRB of modal frequency and damping for both FO cases and ambient conditions as a function of FO frequency with constant local SNR (upper left), as a function of FO frequency with constant local SNR (upper left), as a function of FO frequency with constant global SNR (lower left), as a function of global SNR with constant FO frequency (upper right), and as a function of record length with constant SNR and FO frequency (lower right).

V. Conclusions

Through the derivation and analysis of the CRB on the variance of FO parameters and modal frequency and damping, several interesting observations were made. Arguably the most important is that whenever possible, one should include in their analysis window the FO startup transient. Ongoing work in this area includes a deeper investigation into the mechanisms behind these observations and the implications they may have on system probing. Additionally, these results should be extended to include FO ending transients, along with using the CRBs to benchmark the performance of several recently developed FO estimation and mode meter algorithms.

References

[1] L. Vanfretti, S. Bengtsson, V. S. Perić, and J. O. Gjerde, "Effects of forced oscillations in power system damping estimation," in *Applied Measurements for Power Systems (AMPS), 2012 IEEE International Workshop on*. IEEE, 2012, pp. 1–6.

[2] C. Wang, C. Mishra, K. D. Jones, R. M. Gardner, and L. Vanfretti, "Identifying oscillations injected by inverter-based solar energy sources," in *2022 IEEE Power & Energy Society General Meeting (PESGM)*, 2022, pp. 1–5.

[3] A. Alam et al., "Eastern Interconnection oscillation disturbance January 11, 2019 forced oscillation event," North American Electric Reliability Corporation (NERC), Tech. Rep., December 2019.

[4] L. Dosiek, "On the cramer–rao bound of power system electromechanical mode meters," *IEEE Transactions on Power Systems*, vol. 34, no. 6, pp. 4674–4683, 2019.

[5] Z. Xu and J. W. Pierre, "Initial results for cramer-rao lower bound for forced oscillations in power systems," in *2021 North American Power Symposium (NAPS)*, 2021, pp. 1–5.

[6] Z. Xu, J. W. Pierre, R. Elliott, D. Schoenwald, F. Wilches-Bernal, and B. Pierre, "Cramer-rao lower bound for forced oscillations under multi-channel power systems measurements," in *2022 17th International Conference on Probabilistic Methods Applied to Power Systems (PMAPS)*, 2022, pp. 1–6.

[7] L. Ljung, *System Identification: Theory for the User*, 2nd ed. Upper Saddle River, NJ: Prentice Hall, 1999.

[8] D. Trudnowski, D. Kosterev, and J. Undrill, "PDCI damping control analysis for the western north american power system," in *2013 IEEE Power Energy Society General Meeting*, July 2013, pp. 1–5.